Design Flexibility of a Modular Low-Loss High-Frequency Inductor Structure

Rachel S. Yang, *Student Member, IEEE*, Alex J. Hanson, *Member, IEEE*, Charles R. Sullivan, *Fellow, IEEE*, and David J. Perreault, *Fellow, IEEE*

***Abstract*—Miniaturization and efficiency of power electronics are limited by magnetic components, which are difficult to scale to small size and high frequency (HF). Inductor structures using field shaping, quasi-distributed gaps, and modular construction can achieve low loss at HF (3–30 MHz) without litz wire. For widespread adoption though, these structures must be shown to remain effective across a wide design range and be economical to manufacture. This article investigates the design flexibility of one such previously proposed inductor structure with a modified pot core and demonstrates that this structure can provide excellent performance for a wide range of inductance and power handling requirements using only a few sets of manufactured core pieces. The core pieces used in the modified pot core structure can be scaled by 4× in volume, compared to roughly 2× for conventional core families, and still achieve high performance over a wide design space. Moreover, this approach can achieve about half the loss of conventional designs at HF and, unlike conventional core sets, can provide a range of low-loss form factors with a single family of components. The proposed inductor structure and design approaches, thus, offer new opportunities in the practical production of low-loss HF inductors.**

***Index Terms*—Distributed gap, field shaping, high frequency (HF), inductors, magnetics, skin effect.**

I. Introduction

HIGH-FREQUENCY (HF) operation (3–30 MHz) can enable miniaturization and improved performance of power electronics. At HF, however, magnetic components suffer from HF loss mechanisms, such as skin effect, proximity effect, and hysteresis loss, creating a bottleneck in power electronics development. Recently, studies of losses in commercially available ferrite materials for HF application have identified materials that offer low losses [2], [3] and present opportunities for high-performance inductor designs. To realize the potential of these materials, it is necessary to also consider the effect of the core geometry on HF copper loss, including the effect of fringing fields, leading to approaches such as distributed gaps and field shaping (e.g., [4]–[11]). Such designs and structures have been shown to achieve low loss in example designs.

For a new core structure to be practical beyond use in a one-off custom design, its performance and limitations must be evaluated across a range of design requirements, which can be represented as a region in the 2-D plane of operating power (V × I) and impedance (V/I). Furthermore, to see whether a proposed structure can substantially impact the industry, we must evaluate its flexibility and scalability for addressing a variety of customer needs. One approach is to first consider the range of inductances and power handling capabilities[1] that a single core set of a structure can cover (see Fig. 1). From there, we consider how core set components may be scaled in size to cover adjacent areas of the design space, thereby forming a series of core sets, or core

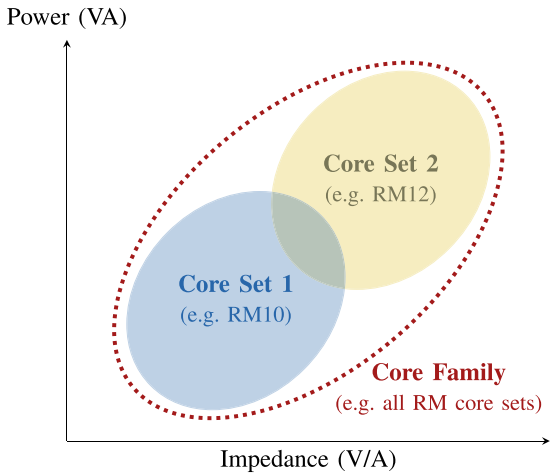

Fig. 1. A single core set at a given loss or thermal limit can cover a certain area of the design space, represented by a range of impedances and power handling capabilities (i.e., V/A ratios and V × A products). A viable series of core sets, or core family, has some overlap in achievable design space, and the most economical family of core sets covers the widest area with the fewest sets.

Manuscript received November 19, 2020; revised March 10, 2021; accepted April 13, 2021. Date of publication April 30, 2021; date of current version July 30, 2021. This work was supported in part by the National Science Foundation under Grant 1609240, in part by the National Science Foundation Graduate Research Fellowship under Grant 1122374, in part by the E.E. Landsman (1958) Fellowship, and in part by the Cooperative Agreement between the Masdar Institute of Science and Technology, Abu Dhabi, UAE, and the Massachusetts Institute of Technology (MIT), Cambridge, MA, USA, under Grant 02/MI/MIT/CP/11/07633/GEN/G/00. This article was presented in part at the 2020 IEEE Applied Power Electronics Conference [1]. Recommended for publication by Associate Editor Q. Li. *(Corresponding author: Rachel S. Yang.)*

Rachel S. Yang and David J. Perreault are with the Massachusetts Institute of Technology, Cambridge, MA 02139 USA (e-mail: rsyang@mit.edu; djperrea@mit.edu).

Alex J. Hanson is with the University of Texas at Austin, Austin, TX 78712 USA (e-mail: ajhanson@utexas.edu).

Charles R. Sullivan is with the Thayer School of Engineering, Dartmouth College, Hanover, NH 03775 USA (e-mail: charles.r.sullivan@dartmouth.edu).

Color versions of one or more figures in this article are available at https://doi.org/10.1109/TPEL.2021.3076774.

Digital Object Identifier 10.1109/TPEL.2021.3076774

[1]This article uses volt-amperes (VA) as the metric for power handling of sinusoidal waveforms at a frequency f, where $\mathrm{VA} = V_{\mathrm{rms}} \cdot I_{\mathrm{rms}} = (2\pi f \lambda) I_{\mathrm{rms}} = \pi f L I^2$ and I is the amplitude of the sinusoidal current.

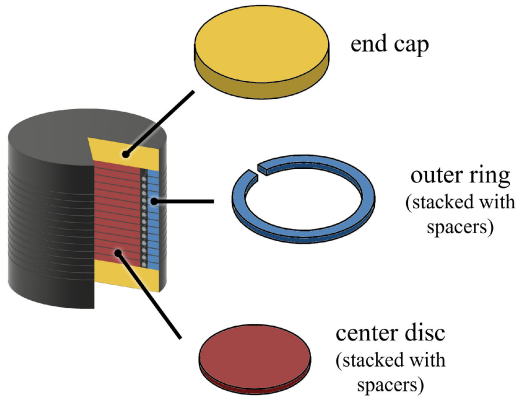

Fig. 2. A single core set of the MP inductor structure is composed of three types of magnetic parts: the center disc, the outer ring, and the end cap. The outer ring may be realized as a ring with a notch cut out to allow for the winding terminations to leave the structure. A stack of center discs with gap spacers form the center post, and a stack of outer rings with gap spacers form the outer shell.

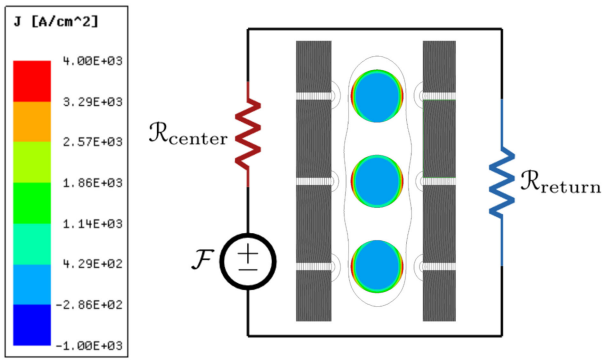

Fig. 3. A section of the winding window in the MP inductor structure illustrating field shaping. The structure balances H fields (shown via black B field lines) on either side of the winding by designing the reluctances in the core center post and return path to be equal. With balanced fields, the current more evenly distributes around the circumference of the conductor through double-sided conduction, thus achieving lower copper loss.

family. If a single core set can cover a wide area, the entire space can be covered by fewer core sets with a larger size scaling factor so that fewer types of parts need to be manufactured.

In [4], a closed-core modular inductor structure using quasi-distributed gaps and field shaping is shown to achieve a high quality factor Q in an example design. This structure is suitable for designs with large ac currents, where the inductor design is limited by loss rather than saturation, e.g., resonant converters, discontinuous conduction mode converters, or boundary conduction mode converters. To achieve high Q, the structure uses a modified pot (MP) core with cylindrical end caps and a carefully designed center post and outer shell, composed of a modular stack of center discs, outer rings, and center and outer gap spacers (see Fig. 2). With this geometry, the MP core implements field shaping to achieve lower copper loss in a single-layer winding through double-sided conduction, where the current more evenly distributes around the circumference of the conductor (see Fig. 3). To do this, the structure balances the reluctances in the core center post and return path, which balances the H fields on either side of the winding.

Due to its low loss and modularity, the MP structure can potentially cover a large design space with a small set of parts, while also providing form factor flexibility. Furthermore, the MP structure has been demonstrated to facilitate the design of extremely high-power-density and high-efficiency power converters operating at HF [12].

In this article, we investigate the design flexibility of the MP structure in [4] by exploring the design space covered by a single core set as well as scaling approaches for core set components. We demonstrate that this structure can indeed cover a wide design space with low loss, that a $4\times$ scaling in volume is a potential approach for creating complimentary core sets (versus $2\times$ in conventional core sets), and that the MP structure substantially outperforms designs based on conventional cores of similar volumes at HF. This article significantly extends the work in [1] by expanding the performance comparisons between MP cores and conventional cores with additional data and analysis. Among other elements, this expansion includes more extensive modeling, analysis, and simulation, as well as a performance comparison of the proposed approach to that achievable with conventional pot cores.

II. Design Flexibility of a Single Core Set

A single *core set* of the MP core is composed of one set of magnetic parts (the end cap, outer ring, and center disc) having a *footprint* defined by the diameter of the end cap. We denote a core set for this type of MP core by MPa, where a is the approximate footprint diameter in millimeters. Due to the modularity of the core set, inductors may be designed with different numbers of magnetic/spacer layers. We specify an inductor configuration that uses core set MPa by MPa-b, where b is the aspect ratio of the height to the diameter, h/D. For example, the MP27 core set has a footprint diameter of 27 mm, from which many inductors can be created. An MP27-1.0 inductor uses the MP27 core set with a stack of magnetic/spacer layers that results in a total height of 27 mm.

In this section, we explore the design flexibility of a single MP core set by investigating its performance across different design requirements. To do this, we used finite element analysis (FEA) simulation to evaluate the inductance and power handling range of the MP27 core set proposed in [4] by adjusting the number of turns in the winding, the number of discs and gaps, and the gap length. For this investigation, the frequency was held constant at 3 MHz. To get a first-order understanding of how the MP inductor's performance changes with volume, a surface temperature rise constraint of $\Delta T \leq 40\ ^\circ\text{C}$ was imposed using a constant heat flux model[2] [13], [14]. With this temperature rise constraint, the allowable loss in an inductor scales with its surface area to account for larger volume inductors being able to dissipate more heat.

[2]This thermal model assumes that power dissipates evenly over the entire surface area of a structure and estimates temperature rise using $P \approx hA\Delta T$, where P is the dissipated power, h is the heat transfer coefficient, A is the surface area of the structure, and ΔT is the change in temperature. Using the MP27-1.0 prototype in [4], we experimentally estimated $h = 10.0\ \text{W}/(\text{m}^2 \cdot\ ^\circ\text{C})$. This first-order thermal model provides a rough understanding of how inductor performance scales with volume, but more precise thermal models may also be used for more in-depth evaluation.

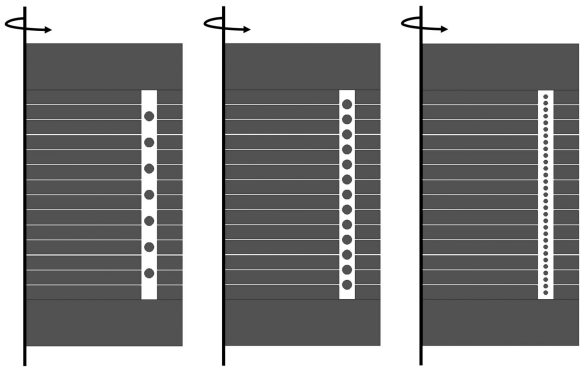

Fig. 4. Core window cross sections for different numbers of turns in a single MP core configuration. As the number of turns changes to vary the inductance, the conductor diameter is also adjusted to appropriately fill the window. For very small number of turns (left), the wire diameter is limited by the window width, leading to large vertical spacing between turns. For very large number of turns (right), the wire diameter is limited by the window height.

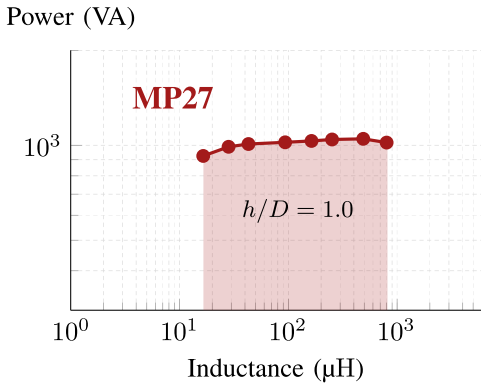

Fig. 5. Simulated maximum power handling curve at $\Delta T = 40$ °C and 3 MHz of the MP27-1.0 configuration. The range of achievable inductor requirements satisfying $\Delta T \leq 40$ °C is the shaded area underneath this curve. The configuration can cover a factor-of-50 range of inductances at ∼1000 VA.

For the computational modeling in this work, we used 2-D cylindrical simulations in ANSYS Maxwell 19.2. The core material used was Fair-Rite 67 (a very low loss NiZn ferrite), and the winding was limited to single-strand round wire. Core loss was estimated using the Steinmetz equation $P_v = k_c f^\alpha B^\beta$ with the parameters $k_c = 0.034$, $\alpha = 1.18$, and $\beta = 2.24$ (for P_v in mW/cm^3, f in Hz, and $\hat{B}$ in T), which were derived using core loss data from [2]. For geometry specifications of all simulated MP inductors in this article, see Appendix A.

A. *Inductance Range*

For a given core geometry, the inductance can be changed via the number of turns and/or the overall gap length. A large deviation in gap length from the optimum, however, can greatly degrade Q by shifting the copper and core loss distribution. Therefore, we focused on the inductance range achievable by only changing the number of turns (and adjusting the conductor diameter accordingly to appropriately fill the window) (see Fig. 4).

To determine the achievable inductance range of a core configuration, we evaluated its maximum power handling capability across inductance at the maximum allowable temperature rise $\Delta T = 40$ °C. For a given configuration with fixed gap length, its maximum power handling should be relatively constant across inductance. To understand why this is true, we consider how the loss of a core configuration behaves across inductance at a constant VA (or energy storage) for a moderate range of turns with reasonable window utilization (see the middle example in Fig. 4). In this case, since the energy storage is constant for a fixed core geometry, the B fields, and thus the core loss, stay fairly constant across inductance. Furthermore, with a single-layer winding, changing the number of turns in the configuration also does not greatly change copper loss. Since the winding only has a single layer, we neglect proximity effect loss in this analysis. At high frequencies where the winding is skin-depth limited, the conduction area roughly scales with wire diameter. Since the total length increases with N and the wire diameter decreases with N to maintain the same vertical window fill, the conductor resistance (R) roughly scales as N^2. Furthermore, to maintain constant peak energy storage, since inductance scales as N^2, the current (i) scales as $1/N$. Thus, as the number of turns varies, the i^2R power loss stays roughly constant. This relatively constant copper loss can also be explained by approximately modeling the single-layer winding as a foil winding, which has a constant sheet current, and thus constant loss, regardless of the number of turns. Therefore, for constant VA and fixed gap length, the loss in the MP inductor structure does not vary greatly with the number of turns across a wide inductance range.

However, for single-strand round wire, the maximum power handling of a configuration drops off for very small N, as the window width restricts the wire diameter for poor vertical window utilization, and for very large N, as winding resistance scales faster than N^2 for wire diameters approaching the skin depth (see Fig. 4). A different wire type, e.g., oval or rectangular, could extend this constant maximum power handling region, as could the introduction of variations in gap length.

In this article, we estimate the achievable inductance range of a core configuration as the range in which it achieves relatively constant power handling at the maximum temperature rise $\Delta T = 40$ °C using single-strand round wire. Thus, our results are conservative; different wire choices could improve performance especially at the extremes of the inductance range.

The analysis for a wide achievable inductance range was verified in simulation using the MP27-1.0 core configuration from [4] (16.6 μH with 13 turns) with single-strand round wire. Fig. 5 plots the achievable inductance range of the MP27-1.0 configuration at the maximum temperature rise $\Delta T = 40$ °C to yield a maximum power handling curve. For a smaller temperature rise, the plotted curve would shift downward on the VA-L plane. Therefore, the range of achievable inductor requirements satisfying $\Delta T \leq 40$ °C for the MP27-1.0 configuration can be roughly represented on the VA-L plane as the shaded area in Fig. 5 with an upper bound defined by the maximum power handling curve. For simplicity, similar figures for the rest of this article will only plot the maximum power handling curve without the shaded region.

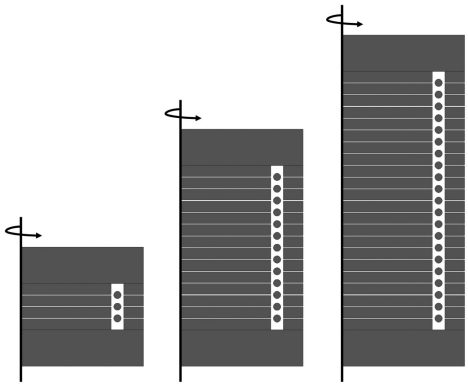

Fig. 6. Examples of different core configurations achievable with a single MP core set. Using only three types of core pieces, the volume of the MP structure can be changed by changing the number of stacked core pieces in the center post and outer shell. Smaller inductors in a given core set, thus, have lower aspect ratios (h/D) than larger inductors.

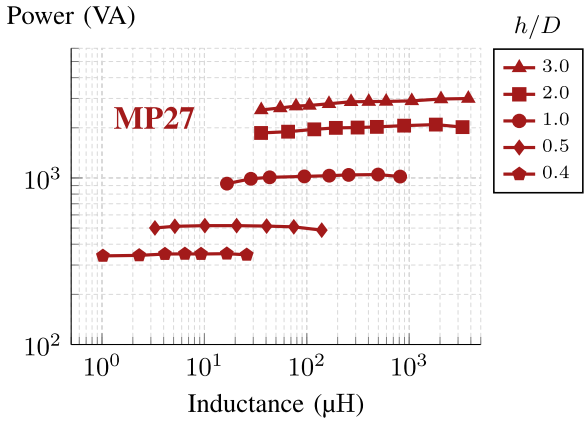

Fig. 7. Simulated maximum power handling curves at $\Delta T = 40\,^{\circ}$C and 3 MHz of the MP27 core set at various volumes, corresponding to different aspect ratios. The power handling of the structure scales with volume (or aspect ratio) by changing the number of stacked core pieces in the center post and outer shell. For the plotted range of aspect ratios, this core set can achieve a factor-of-10 range in power handling. Each curve also achieves a wide inductance range.

From Fig. 5, we can see that the MP27-1.0 configuration achieves relatively constant maximum power handling capability across inductance. At a high power handling threshold of $\sim$1000 VA, this core configuration can cover at least a factor-of-50 range of inductances. Since the performance analysis across inductance is not specific to this configuration, we can expect a similarly wide coverage of inductance for other configurations, as confirmed in later sections.

B. Power Handling Range

For a given MP core set, the volume of the inductor structure, and thus its power handling capability, can be changed with relatively fine granularity via the number of stacked core pieces in the center post and outer shell (see Fig. 6). The aspect ratio (h/D) of the structure also scales linearly with volume.

To evaluate the power handling range of the MP27 core set, structures with different volumes (and aspect ratios) were simulated with FEA across a range of inductances at the maximum allowable temperature rise $\Delta T = 40\,^{\circ}$C (see Fig. 7). All simulated core configurations used symmetric core stacking, where the center post and outer shell have the same number of stacked core pieces. As in Section II-A, designs with each core configuration (i.e., core set size and selected aspect ratio) maintained the same gap pitch, or spacing between core discs, across inductance sweeps. However, the gap pitch was varied between core configurations to achieve total gap lengths that roughly optimized core and copper loss distribution in each configuration.

The plotted region in Fig. 7 coarsely represents the design space that the MP27 core set can reasonably cover. Varying the number and diameter of the turns allows each core configuration to cover a wide range of inductances[3] with high performance, as predicted in Section II-A. As expected, taller inductors in a given core set can also process more power because they have greater volume. For a reasonable range of aspect ratios ($0.4 \leq h/D \leq 3.0$), the core set can accommodate nearly a factor of 10 in power at $\Delta T = 40\,^{\circ}$C using only three distinct core components. The lower bound of this range ($h/D = 0.4$) is set by the height of two stacked core pieces with a single gap in the center post and outer shell, while the upper bound ($h/D = 3.0$) is set by practical considerations of desired inductor shapes.

III. Approaches for Constructing an Economical and High-Performance MP Core Set Family

Next, we used FEA simulation to explore approaches for scaling MP core set sizes in the same way that conventional cores are scaled to yield a core family, e.g., RM10, RM12, RM14, etc. These scaling approaches should economically cover a wide design space with a few core sets and also maintain high performance across design requirements.[4] For continuous coverage, adjacent core set sizes should also have an overlap in their achievable design spaces.

To determine appropriate scaling approaches, we consider how the MP inductor structure's performance changes across aspect ratio with symmetric core stacking. As shown in [4], at a single design volume, the MP structure achieves optimum Q at an aspect ratio of $h/D \approx 1$, with Q falling off slowly from this optimum. The MP core set family with the greatest performance would, thus, be solely composed of MP core configurations at $h/D = 1$. In this case, the family would achieve the optimum power handling capability of the MP structure across all volumes. However, doing so would be costly; every design volume would require a separate core set.

To help reduce manufacturing needs, a single MP core set can be used to cover a range of design volumes by varying its core

[3]The plotted inductance ranges shift to the right with taller inductors due to the limitation of using single-strand round wire. Taller inductors with taller window heights can accommodate more turns for a given wire diameter, allowing them to achieve greater inductances than shorter inductors. Conversely, shorter inductors continue to well-utilize their window height at fewer turns than taller inductors, allowing shorter inductors to achieve lower inductances.

[4]This section focuses on the technical performance of scaling approaches. For discussion on manufacturing and practical considerations, see Appendix B.

TABLE I
GEOMETRY OF VARIOUS MP CORE SETS

	MP17	MP21	MP27	MP33	MP42
Volume Scale Factor	0.25	0.5	1.0	2.0	4.0
Total Diameter	16.75 mm	21.1 mm	26.9 mm	33.5 mm	42.2 mm
Center Post Radius	5.75 mm	7.2 mm	9.9 mm	12.0 mm	15.5 mm
Window Width	1.2 mm	1.65 mm	1.4 mm	1.7 mm	2.1 mm
End Cap Height	2.5 mm	3.0 mm	4.0 mm	5.0 mm	6.0 mm
Core Disc/Ring Height	0.83 mm	1.16 mm	1.18 mm	1.18 mm	1.46 mm

stacking height (and thus aspect ratio), as in Section II-B. In this case, each core set is optimized at $h/D = 1$ to achieve field balancing for double-sided conduction, which reduces winding loss by better utilizing the wire surface for conduction (see Fig. 3). To do this, the structure balances the reluctances in the center post and return path (outer shell and fringing field) at $h/D = 1$. For taller or shorter core configurations in each core set, though, the constraint of fixed core piece geometries leads to a lower Q at these design volumes compared to a custom MP core design at $h/D = 1$ having the same volume. As the number of stacked core pieces changes, the reluctances in the center post and outer shell scale similarly. However, the fringing field reluctance ($\mathcal{R}_{\text{fringe}} \approx 0.9/(\mu_0 \pi r_t)$) is fixed by the footprint of the core set and is not significantly affected by the height [15]. So, for symmetric core stacking[5] in the center post and outer shell, the reluctances in the center post and return path cannot remain balanced, leading to field imbalance and loss of perfect double-sided conduction for $h/D \neq 1$.

To ensure high performance across all design volumes, core set footprints should then be scaled when a core set greatly underperforms the adjacent core set, i.e., when the tallest inductor in a core set is outperformed by the shortest inductor of the next largest core set. To help determine this scaling, we evaluated the simulated maximum power handling at $\Delta T = 40\,^{\circ}\text{C}$ of different MP core sets across a reasonable range of aspect ratios ($0.4 \leq h/D \leq 3.0$) and compared the performance at each volume to that of custom MP structures at $h/D = 1$, which achieve the optimum MP power handling capability. The different core set footprints were scaled in volume from the MP27-1.0 configuration, with each total dimension scaled equally (see Table I). For example, a core set footprint is scaled by $4\times$ in volume if its $h/D = 1.0$ configuration is $4\times$ the volume of the MP27-1.0 configuration, with the volume of inductors in both core sets varying with h/D. The core set geometry for each footprint was designed to roughly optimize performance at $h/D = 1$, using the design guidelines and the example design algorithm in [4].

Fig. 8 plots the maximum power handling of five different MP core sets across volume, normalized to the optimum power handling capability at each volume. As shown in this figure, each MP core set achieves near optimum power handling for aspect ratios $h/D \geq 1$. While the Q of the MP structure declines from optimum for $h/D > 1$, taller structures can better dissipate heat, as their surface area to volume ratio is larger than that of a structure with a "square" aspect ratio ($h/D = 1$). Thus, for a constant temperature rise constraint, MP structures can continue to perform near optimum for large aspect ratios.

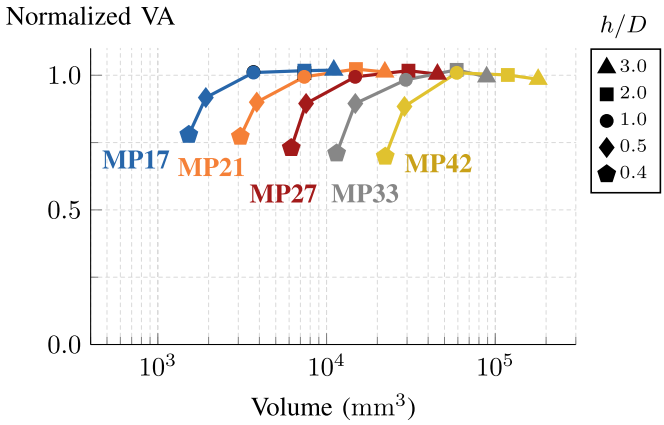

Fig. 8. Simulated normalized power handling curves across volume for various MP core sets at $\Delta T = 40\,^{\circ}\text{C}$ and 3 MHz. The power handling capability of each core configuration is normalized to the optimum power handling at each volume. For $h/D \geq 1$, each core set has roughly optimum power handling capability. For $h/D < 1$, the performance drops off slowly, with the smallest aspect ratio $h/D = 0.4$ still achieving ~70% of the optimum VA.

For $h/D < 1$, the performance of each core set begins to drop off. For shorter structures in a core set, the Q falls from optimum more quickly than the surface-area-to-volume ratio increases. Since the end cap heights in each core set are fixed, shorter structures have less volume for the "active" section (everything but the end caps), where flux links the winding, which degrades the Q. However, the drop-off in power handling performance is relatively slow. Even at the smallest possible aspect ratio $h/D = 0.4$, composed of two core pieces with a single gap, the performance is still at least ~70% of the optimum VA. Therefore, a single core set can maintain high performance for a wide range of aspect ratios and volumes, suggesting that core set components can have relatively large scaling factors without reducing performance.

A. 2× Volume Scaling

Typical industry-standard closed cores, e.g., RM or pot cores, are scaled in size by $2\times$ in volume [16], [17]. Therefore, we first evaluated the performance of an MP core family with core set components having this scaling factor (with each dimension

[5]Asymmetric core stacking in the center post and outer shell is possible if their total heights are the same. With this type of stacking, perfect double-sided conduction may be achieved, but with ramifications to core loss as B fields in the center post and outer shell redistribute. Since asymmetric stacking has additional nontrivial considerations, it is not included in this article.

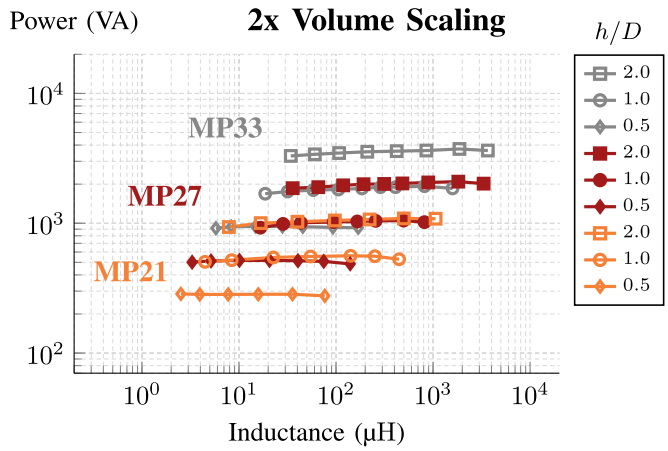

Fig. 9. $2\times$ volume scaling: simulated maximum power handling curves at $\Delta T = 40$ °C and 3 MHz of the MP21 (orange), MP27 (red), and MP33 (gray) core sets at various aspect ratios. The three core sets have large overlap regions for great form factor flexibility.

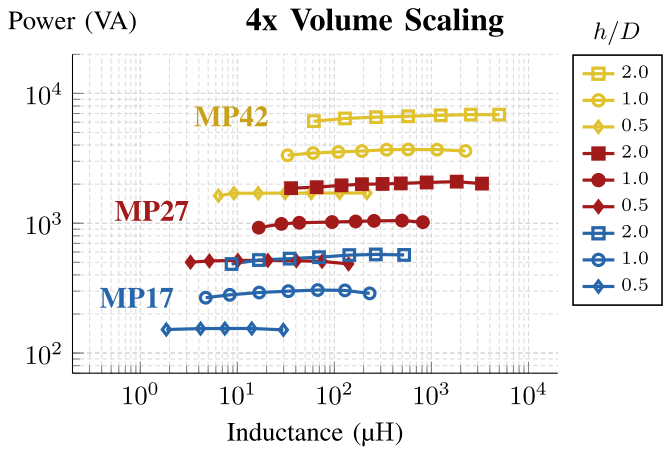

Fig. 10. $4\times$ volume scaling: simulated maximum power handling curves at $\Delta T = 40$ °C and 3 MHz of the MP17 (blue), MP27 (red), and MP42 (yellow) core sets at various aspect ratios. Compared to $2\times$ volume scaling (see Fig. 9), these three core sets cover a wider design space, but still have overlap regions for some form factor flexibility.

scaled equally). In Fig. 8, for example, such a core family would include all of the core sets shown. In this family, each design volume has multiple high-performance core set options, suggesting that core sets scaled by $2\times$ in volume can have large overlaps in their achievable design space.

To examine these overlaps in detail, Fig. 9 plots the achievable design space for three adjacent core sets with components scaled by $2\times$ in volume: MP21, MP27, and MP33 from Fig. 8. For an aspect ratio range of $0.5 \leq h/D \leq 2.0$, these core sets cover at least three orders of magnitude in inductance and a factor of 15 in maximum power handling with large overlaps in design space as expected, providing great form factor flexibility. Height-constrained applications can use larger footprint core sets with smaller aspect ratios, while footprint-constrained applications can use smaller footprint core sets with taller aspect ratios. As shown in Fig. 9, with $2\times$ volume scaling, any given volume has at least two form factor options: one at a smaller footprint with taller aspect ratio and one at a larger footprint with shorter aspect ratio. At the volume of MP27-1.0, two additional form factors exist, MP21-2.0 and MP33-0.5, for a total of three form factors.

B. $4\times$ Volume Scaling

Since scaling core set components by $2\times$ in volume yields large overlaps in achievable design space, a larger scaling factor could produce a more economical MP core family that uses fewer core sets to cover a wide design space at low loss. From Fig. 8, a suitable MP core family could be composed of core sets that span an aspect ratio range from $h/D = 0.5$ to $h/D > 3.0$. However, even though core sets with a high aspect ratio can handle near optimum VA at $\Delta T = 40$ °C, structures taller than $h/D = 2.0$ become undesirable in terms of shape and achievable Q. Thus, we choose the range of $0.5 \leq h/D \leq 2.0$ with adjacent core sets overlapping in volume at these boundaries. Such a family corresponds to core set components being scaled by $4\times$ in volume (with each dimension scaled equally), e.g., MP17, MP27, and MP42 in Fig. 8. At $h/D = 0.5$, MP core sets maintain high performance at ~90% of the optimum VA.

Scaling MP core set footprints by $4\times$ in volume covers a wider design space than the typical industry-standard scaling factor of $2\times$ in volume (see Fig. 10). Just three adjacent core sets with $4\times$ volume scaling can cover at least three orders of magnitude in inductance and a factor of 45 in maximum power handling. Furthermore, at the overlap regions between core sets (MP17-2.0 and MP27-0.5; MP27-2.0 and MP42-0.5), adjacent core sets have comparable performance for similar volume, allowing for some form factor flexibility.

C. Other Volume Scaling

Other scaling factors for MP core sets can also be considered. For example, MP core set components could be scaled by factors between $2\times$ and $4\times$ in volume. Sliding the scaling factor along this scale would change the density of core sets on the VA-L plane, thus trading off economic coverage of the design space with form factor flexibility. Scaling factors larger than $4\times$ could also be considered, but would result in no overlap of maximum power handling capabilities between core sets (with $0.5 \leq h/D \leq 2.0$). Designs in between core sets would then use cores from the larger core set for suboptimal power density, similar to what is done with conventional cores.

In summary, we find that scaling volume by a factor of 4 between adjacent core sets is a good choice to enable coverage of a broad range of inductance and power levels at low loss with a modest number of components. The absolute sizes of the MP17, MP27, and MP42 core pieces detailed in Table I can form one basis for a broadly spanning set of cores.

TABLE II
SPECIFICATIONS FOR SOLID-WIRE MP INDUCTOR PROTOTYPES

Core	L	# of Core Pieces	Total Gap Length	N	Wire Gauge
MP17-1.0	8.1 µH	13	0.96 mm	12	22 AWG
MP17-2.0	15.7 µH	31	3.00 mm	25	22 AWG
MP27-0.5	16.7 µH	4	0.60 mm	9	27 AWG
MP27-1.0	13.8 µH	14	2.08 mm	13	20 AWG

Fig. 11. Inductor prototypes with core configurations (left to right): MP17-1.0, MP17-2.0, MP27-0.5, and MP27-1.0.

IV. EXPERIMENTAL RESULTS FOR THE MP17 AND MP27 CORE SETS

We validated the simulated performance of the MP17 and MP27 core sets at 3 MHz with four inductor prototypes spanning three different volumes using solid-core wire: MP17-1.0, MP17-2.0, MP27-0.5, and MP27-1.0 (see Table II and Fig. 11), i.e., two designs at the optimal aspect ratio (∼1.0) [4] and two designs of similar volume but different footprint.[6] The use of litz wire to improve the Q of these prototypes was also demonstrated through the construction and measurement of four inductors having the same set of sizes but using litz wire (see Table IV).

A. *Q* Measurements Validate Simulations

Using the resonant measurement approach for high Q from [4],[7] large-signal Q measurements of the four solid-wire inductor prototypes were taken at their respective simulated maximum VA level, determined by simulated loss and a calculated temperature rise of $\Delta T = 40$ °C. For each VA level, the inductor was operated at a current corresponding to the desired VA, i.e., $I = \sqrt{\mathrm{VA}/(\pi f L)}$. The measured quality factors of the four prototypes agreed with the simulated ones, validating the simulated loss models (see Table III). The MP17-2.0 and MP27-0.5 inductors, which have the same volume, also had comparable measured quality factors (within 15% of each other), verifying an overlap in design space at high performance between the two core sets.

[6]The prototypes were built using the same construction process as in [4], except the outer shell for the MP17 prototypes was constructed from a single stack of outer rings (see Fig. 2) instead of three stacked sections.

[7]This measurement approach operates a series LC circuit at resonance to estimate the Q of the inductor at high drive levels. To more accurately measure high Q at HF, the approach compensates for loss in the capacitor equivalent series resistances and uses a capacitor divider to minimize probe loss and loading.

TABLE III
SIMULATED AND MEASURED RESULTS OF MP17 AND MP27 INDUCTORS AT 3 MHZ FOR PROTOTYPES DESCRIBED IN TABLE II

Core	L (sim)	L (meas)	VA	Q (sim)	Q (meas)
MP17-1.0	8.1 µH	6.8 µH	280	520	520
MP17-2.0	15.7 µH	12.9 µH	520	590	590
MP27-0.5	16.7 µH	15.8 µH	520	570	500
MP27-1.0	13.8 µH	13.4 µH	910	680	690

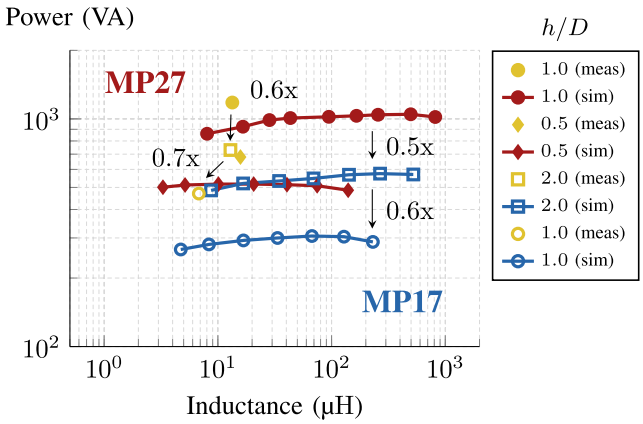

Fig. 12. 4× volume scaling: experimental power handling capability of the prototype MP inductors (yellow) at $\Delta T = 40$ °C and 3 MHz compared to simulated results of the MP17 (blue) and MP27 (red) core sets. The prototype inductors achieved similar scaling of power handling with volume compared to simulations using a constant heat flux model. Both core sets also experimentally achieved similar power handling at the same volume (MP17-2.0 versus MP27-0.5), agreeing with simulations.

B. Experimental Power Handling Capabilities Scale Similarly to Simulations

To experimentally verify how power handling scales with core set sizes, the four prototype inductors were tested at $\Delta T = 40$ °C, achieved by adjusting the large-signal excitation amplitude.[8] For this verification, we evaluated the relative scaling of VA handling rather than the absolute VA handling values.

As shown in Fig. 12, the prototype inductors achieved similar relative scaling of power handling compared to simulations using a constant heat flux model. The MP17 and MP27 core sets also had comparable power handling (within 7%) at the same volume (MP17-2.0 versus MP27-0.5), thus verifying an overlap in performance achievable with the two core sets. These results suggest that a 4× volume scaling factor may be effective for covering a wide range of inductor requirements with a restricted number of MP core sets.

The slightly slower scaling of VA handling with volume in the experimental results compared to simulation can be attributed to second-order effects not accounted for in the constant heat flux model, which assumes that for a fixed temperature rise, the allowable loss scales proportionally with the inductor's surface area. In reality, smaller volume inductors are better at transferring heat, so they can handle more power than the constant heat

[8]40 °C was the average surface temperature rise of the inductors, measured using a FLIR E6 thermal camera at different angles.

TABLE IV
MEASURED RESULTS OF MP17 AND MP27 INDUCTORS WITH LITZ WIRE AT 3 MHZ

Core	Wire	L	VA	Q
MP17-1.0	180/48 litz	6.8 µH	280	700
MP17-2.0	300/48 litz	13.5 µH	520	780
MP27-0.5	100/48 litz	15.5 µH	520	610
MP27-1.0	450/48 litz	12.6 µH	910	960

flux model allows, which is why the experimental VA handling scales down slightly slower than the simulated VA handling.

C. Litz Wire Can Improve Performance of MP Inductors

One major advantage of the MP core type is that it does not require litz wire to achieve high performance, making it potentially scalable to frequencies higher than 3 MHz, where litz wire becomes less practical. Experimental evidence in [4] shows the MP inductor achieving high performance at up to 5.5 MHz without litz wire. Still, it is worth investigating if litz wire can further improve the performance of MP inductors at frequencies where litz wire remains practical (less than ∼4 MHz, where the skin depth in copper equals the diameter of 48-AWG strands).

Litz wire versions of all four MP inductor prototypes were constructed using the same core geometry and number of turns as the solid-wire prototypes (see Table II). Strands of 48 AWG were used, as this wire gauge represents a good balance between cost and power loss at 3 MHz. The optimum number of strands for each inductor was determined using the simplified design method for litz wire [18] to roughly estimate power loss. Readily available litz wire near the optimum design that fit in the core window was then used.

At 3 MHz, litz wire improved the Q of the MP prototypes by ∼20–40% (see Table IV). The MP27-0.5 prototype had less improvement in Q with litz compared to the improvements in the other prototypes because the overall wire diameter was greatly restricted by the window height, leading to poor horizontal window utilization. Nevertheless, the improvements in Q for all four prototypes suggest that even lower loss inductor designs can be achieved by utilizing both litz wire and the MP inductor structure.

V. COMPARISON OF MP AND CONVENTIONAL CORES

To further highlight the benefits of the MP cores, we compared their performance with that of similar conventional cores. Since pot cores have the same cylindrical closed-core shape as MP cores, we first compared FEA simulations of the MP cores to those of standard pot cores using the same core material, Fair-Rite 67. For experimental comparisons, though, we were limited by the availability of cores in this material and instead compared to EQ cores, which are similar in shape to pot cores with a cylindrical center post and partially enclosed cylindrical winding window.

For all comparisons, conventional cores were chosen if they had a similar box volume (core volume including gap length) to one of the four MP prototypes in Section IV. All conventional core designs were roughly optimized for 3 MHz using a MATLAB script that modeled core loss with the Steinmetz equation [19] and winding loss with Dowell's equation [20]. For designs using litz wire, the optimum number of strands for 48-AWG litz was determined using the online LitzOpt software [21], based on the algorithm described in [22]. Readily available litz wire near the optimum design was then used. Both pot core and EQ inductors were gapped in the center post and outer shell/legs, and the windings were centered in the window to reduce fringing field loss from the gaps.

TABLE V
SPECIFICATIONS FOR SIMULATED POT CORE INDUCTORS

Core	L	Gap Length	N	Wire
P30/19	14.3 µH	2.2 mm	15	20 AWG solid
P18/11/I	8.3 µH	0.7 mm	13	24 AWG solid

TABLE VI
SIMULATED RESULTS OF POT CORE AND MP INDUCTORS AT 3 MHZ

	Core	L	Q
14 800 mm^3	P30/19	14.3 µH	380
910 VA	MP27-1.0	13.8 µH	680
3700 mm^3	P18/11/I	8.3 µH	360
280 VA	MP17-1.0	8.1 µH	520

A. MP Core Set Outperforms Pot Cores in Simulation

Two standard pot core sizes[9] using solid-core wire were simulated: P30/19 (30 mm diameter, 19 mm height), which has the same box volume as MP27-1.0, and P18/11/I, which has the same box volume as MP17-1.0 (see Table V).

As shown in Table VI, for each design volume and corresponding VA operating point, the MP inductors achieved substantially higher Q than the pot core inductors in simulation. The larger volume MP inductor improved Q by $1.8\times$, and the smaller volume MP inductor improved Q by $1.4\times$. An example set of field plots comparing the MP27-1.0 and P30/19 inductors is shown in Fig. 13.

We can also see the improved performance of the MP inductors over the pot core inductors by comparing their simulated maximum power handling capabilities. For this comparison, we looked at MP cores from MP17-1.0 to MP27-1.0 and all standard pot core sizes within the same range of volumes (3700–14 800 mm^3). As shown in Fig. 14, at $\Delta T = 40$ °C, the pot core inductors achieved lower VA handling than the MP inductors. In particular, when comparing inductors having the same volume (MP27-1.0 versus P30/19; MP17-1.0 versus P18/11/I), the MP inductors achieved at least $1.6\times$ greater power handling than pot core inductors. Additionally, the P30/19 inductor achieved the same power handling as MP inductors at half the volume (MP27-0.5 and MP17-2.0), further indicating the improved performance potential of MP inductors over conventional pot core inductors.

[9]The P/I version of P18/11 (without a center hole) was used for maximum available core area. P30/19, however, does not have a standard P/I version.

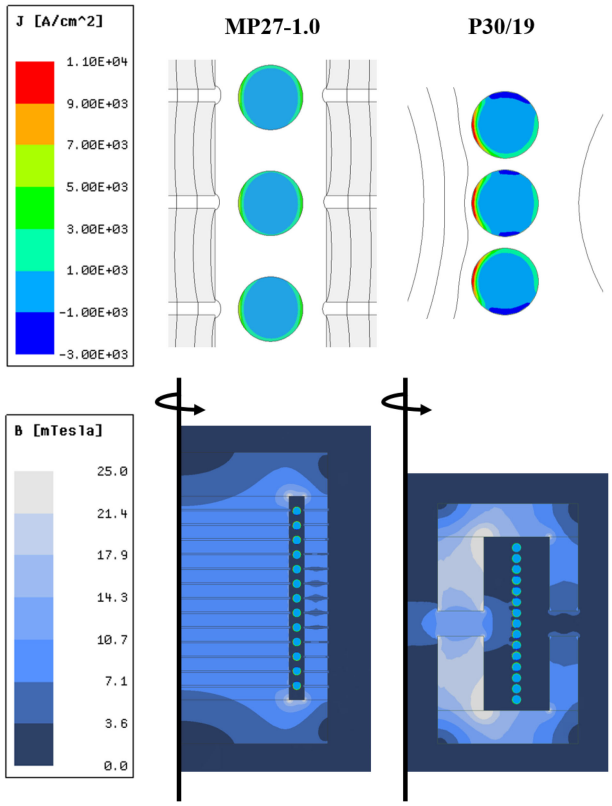

Fig. 13. Field plots comparing an example MP inductor (MP27-1.0, left) with a pot core inductor (P30/19, right) at the same volume and VA level (see Table VI for corresponding simulation results). The MP inductor achieves low copper loss through double-sided conduction by balancing the H fields (shown as black flux lines) on either side of the winding, whereas the pot core inductor sees single-sided conduction due to imbalanced H fields. The MP inductor also achieves low core loss through roughly even distribution of B fields, whereas the pot core inductor sees unevenly distributed B fields for greater core loss in the center post. The distributed gap in the MP inductor reduces leakage and thus maintains more constant flux density along the length of the center post and outer shell. Having a gap near the top of the center post also helps spread flux over the full gap region, reducing flux crowding in corners.

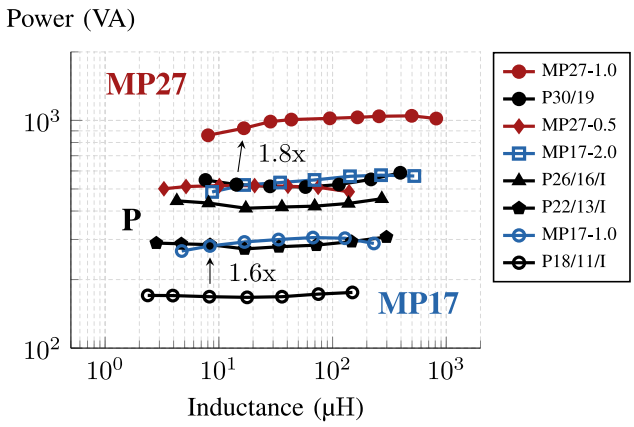

Fig. 14. Simulated power handling capability of MP (red, blue) and pot core (black) inductors with solid wire at $\Delta T = 40\,^{\circ}\mathrm{C}$ and 3 MHz spanning the same range of volumes from 3700 to 14 800 mm^3. When comparing inductors having the same volume (MP27-1.0 versus P30/19; MP17-1.0 versus P18/11/I), the MP inductors achieved at least $1.6\times$ greater power handling than the pot core inductors. The MP inductors also achieved the same power handling as the P30/19 inductor at half the volume.

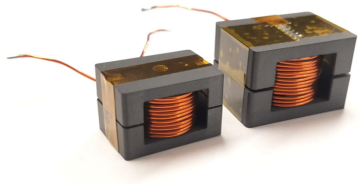

Fig. 15. Inductors built using the commercial EQ core series (left to right): EEQ20/13 and EEQ25/16.

TABLE VII
SPECIFICATIONS FOR EEQ INDUCTORS

Core	L	Gap Length	N	Wire
EEQ25/16	16.5 μH	0.66 mm	14	22 AWG solid
EEQ25/16	16.1 μH	0.66 mm	14	180/48 litz
EEQ20/13	7.8 μH	0.51 mm	11	22 AWG solid
EEQ20/13	7.7 μH	0.51 mm	11	180/48 litz

TABLE VIII
MEASURED RESULTS OF EEQ AND MP INDUCTORS AT 3 MHZ

		solid wire		litz wire	
	Core	L	Q	L	Q
7400 mm^3 520 VA	EEQ25/16	16.5 μH	280	16.1 μH	340
	MP27-0.5	15.8 μH	500	15.5 μH	610
	MP17-2.0	12.9 μH	590	13.5 μH	780
3700 mm^3 280 VA	EEQ20/13	7.8 μH	270	7.7 μH	370
	MP17-1.0	6.8 μH	520	6.8 μH	700

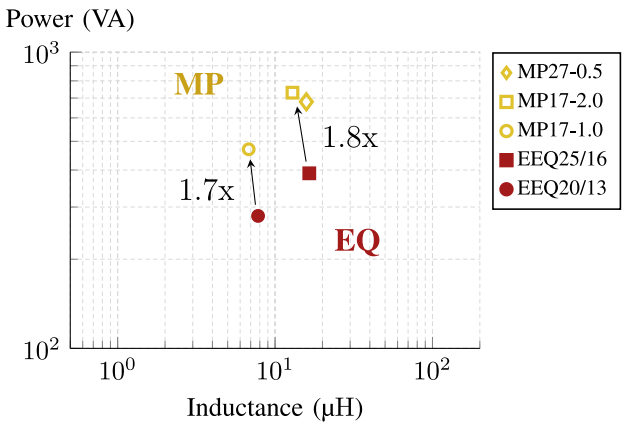

Fig. 16. Experimental power handling capability of MP (yellow) and EEQ (red) prototype inductors with solid wire at $\Delta T = 40\,^{\circ}\mathrm{C}$ and 3 MHz. At a given volume, the MP inductors achieved greater power handling than the EQ inductors.

B. MP Core Set Experimentally Outperforms EQ Cores

To experimentally compare with industry-standard core sets, we designed inductors using EQ cores of the same core material, Fair-Rite 67 (see Fig. 15). Two EQ core sizes were chosen: EEQ25/16 (25 mm long, 16 mm tall), which has the same box volume as MP17-2.0 and MP27-0.5, and EEQ20/13, which has the same box volume as MP17-1.0. Both solid-core and litz wire designs were built using these two EQ core sizes (see Table VII).

As shown in Table VIII, the proposed MP inductors achieved substantially higher Q than the EQ inductors at each design volume for both solid wire and litz wire designs. With solid wire, the MP prototypes improved Q by at least $1.8\times$ compared to EQ inductors at the same volume. With litz wire, MP inductors also improved Q by at least $1.8\times$ compared to EQ inductors at the same volume. At a given volume, the solid-wire MP inductors even substantially outperformed EQ inductors with litz wire.

The improved performance of MP inductors over EQ inductors can also be seen by considering the inductors' power handling capabilities at a fixed temperature rise. As shown in Fig. 16, at $\Delta T = 40\ ^\circ\text{C}$, the MP inductors experimentally achieved at least $1.7\times$ greater power handling than EQ inductors of the same volume.

VI. Conclusion

The MP inductor structure, previously proposed in [4], has great design flexibility due to its modular structure and single-layer winding, making it a potential solution for low-loss HF inductor design. Many different structures can be constructed from a single core set by changing the number of stacked core pieces in the center post and outer shell. A wide range of inductor requirements can, thus, be achieved from a small number of core set components. One possible approach to sizing MP core sets is to scale footprints to achieve $4\times$ scaling in volume; this yields large continuous coverage of the design space at low loss. With this approach, the proposed structure and design techniques can address the design of low-loss HF inductors across a wide range of requirements.

Appendix A
Geometry of Simulated MP Inductors

Tables IX–XIII include geometry details for all simulated MP inductors in this article. Dimensions for each MP core set are listed in Table I. The geometry for each core set was designed to roughly optimize performance at $h/D = 1$, using the design guidelines and example design algorithm in [4].

TABLE IX
Geometry for Simulated MP27 Core Set Inductors in Figs. 5, 7–10, 12, and 14

Core	# of Core Pieces	Total Gap Length	Range of N	Range of Wire Diameters
MP27-3.0	55	7.00 mm	33–340	0.80–0.13 mm
MP27-2.0	35	4.50 mm	28–270	0.80–0.10 mm
MP27-1.0	14	1.48 mm	13–91	0.80–0.12 mm
MP27-0.5	4	0.60 mm	4–26	0.80–0.12 mm
MP27-0.4	2	0.50 mm	2–10	0.80–0.17 mm

TABLE X
Geometry for Simulated MP17 Core Set Inductors in Figs. 8, 10, 12, and 14

Core	# of Core Pieces	Total Gap Length	Range of N	Range of Wire Diameters
MP17-3.0	50	3.40 mm	29–133	0.64–0.20 mm
MP17-2.0	31	2.70 mm	18–140	0.64–0.12 mm
MP17-1.0	13	0.91 mm	9–63	0.64–0.11 mm
MP17-0.5	4	0.40 mm	4–16	0.64–0.14 mm
MP17-0.4	2	0.26 mm	2–8	0.58–0.15 mm

TABLE XI
Geometry for Simulated MP21 Core Set Inductors in Figs. 8 and 9

Core	# of Core Pieces	Total Gap Length	Range of N	Range of Wire Diameters
MP21-3.0	45	5.20 mm	27–250	1.00–0.14 mm
MP21-2.0	29	3.10 mm	15–175	1.00–0.13 mm
MP21-1.0	12	2.35 mm	8–80	1.00–0.11 mm
MP21-0.5	4	0.40 mm	4–22	0.76–0.14 mm
MP21-0.4	2	0.50 mm	3–10	0.56–0.17 mm

TABLE XII
Geometry for Simulated MP33 Core Set Inductors in Figs. 8 and 9

Core	# of Core Pieces	Total Gap Length	Range of N	Range of Wire Diameters
MP33-3.0	68	10.5 mm	33–250	1.00–0.22 mm
MP33-2.0	42	7.40 mm	27–280	1.00–0.12 mm
MP33-1.0	18	2.21 mm	13–120	1.00–0.12 mm
MP33-0.5	5	0.90 mm	5–27	0.82–0.15 mm
MP33-0.4	2	0.65 mm	3–14	0.60–0.13 mm

Appendix B
Practical Considerations of the MP Core Set

To understand whether a proposed structure can substantially impact the industry, not only must its technical performance be evaluated, but its practical production aspects must also be considered. This article thus far has largely focused on evaluating the former for the MP core, demonstrating its design flexibility and scalability as well as its improved performance compared to conventional cores. In this appendix, we begin probing the practical considerations of the MP core. This discussion is intended to provide some initial thoughts on this topic and not a final solution.

Gap Pitch: In this article, the gap pitch, adjusted via the spacing between core discs, was allowed to change between MP core configurations to provide flexibility for loss optimization. To limit the number of distinct core pieces in a core set, changes in gap pitch were implemented by fixing the core disc thickness and changing gap lengths accordingly. This approach to changing gap pitch could be implemented in manufacturing MP core stacks to provide flexibility in design and loss optimization, but would add a layer of complexity in the manufacturing process. To simplify this process, another option for core stack implementation could be to hold the gap pitch constant across all core stacking configurations at the expense of design flexibility. However, the impact of this approach on performance would need to be investigated in more detail.

Surface Losses: In some quasi-distributed designs using MnZn ferrite, increased surface losses have been observed in the multigap section of the core, likely due to mechanical stresses incurred during the machining process [23]. However, for the MP prototypes in this article, the agreement in simulated and measured quality factors suggest that this effect is minimal in these particular prototypes, which use a NiZn ferrite. Therefore,

TABLE XIII
GEOMETRY FOR SIMULATED MP42 CORE SET INDUCTORS IN FIGS. 8 AND 10

Core	# of Core Pieces	Total Gap Length	Range of N	Range of Wire Diameters
MP42-3.0	70	14.0 mm	47–340	1.00–0.21 mm
MP42-2.0	44	8.50 mm	31–280	1.00–0.16 mm
MP42-1.0	18	3.94 mm	17–140	1.07–0.13 mm
MP42-0.5	5	1.40 mm	5–29	1.00–0.18 mm
MP42-0.4	2	1.00 mm	3–20	0.78–0.12 mm

while surface loss effects should be considered, they may only play a large role in certain materials and/or machining processes.

Electromagnetic Compatibility: To achieve reduced conduction loss in the windings through double-sided conduction, the MP structure necessarily has mmf drops on both the inside and outside surfaces of the windings and has associated fringing fields outside of the component. In this regard, the fringing fields from this inductor structure may be expected to fall somewhere between that of a pot core with a center post gap (highly shielded) and that of a dumbbell core with an outer gap.

Turn Spacing: While constructing single-layer windings is a relatively straightforward process (e.g., by using a coil winding machine), additional care would be needed to obtain the desired turn-to-turn spacing, set by vertical window fill guidelines in [4]. This could be achieved through special configuration in the winding setup or through appropriate insulation thickness on the winding.

ACKNOWLEDGMENT

The authors would like to thank Fair-Rite for manufacturing the magnetic core pieces used in the prototypes.

REFERENCES

[1] R. S. Yang, A. J. Hanson, C. R. Sullivan, and D. J. Perreault, "Application flexibility of a low-loss high-frequency inductor structure," in *Proc. IEEE Appl. Power Electron. Conf. Expo.*, 2020, pp. 168–175.
[2] A. J. Hanson, J. A. Belk, S. Lim, C. R. Sullivan, and D. J. Perreault, "Measurements and performance factor comparisons of magnetic materials at high frequency," *IEEE Trans. Power Electron.*, vol. 31, no. 11, pp. 7909–7925, Nov. 2016.
[3] Y. Han, G. Cheung, A. Li, C. Sullivan, and D. Perreault, "Evaluation of magnetic materials for very high frequency applications," *IEEE Trans. Power Electron.*, vol. 27, no. 1, pp. 425–435, Jun. 2011.
[4] R. S. Yang, A. J. Hanson, B. A. Reese, C. R. Sullivan, and D. J. Perreault, "A low-loss inductor structure and design guidelines for high-frequency applications," *IEEE Trans. Power Electron.*, vol. 34, no. 10, pp. 9993–10005, Oct. 2019.
[5] Z. Ouyang and M. A. E. Andersen, "Overview of planar magnetic technology-fundamental properties," *IEEE Trans. Power Electron.*, vol. 29, no. 9, pp. 4888–4900, Sep. 2014.
[6] S. Lu, C. Ding, Y. Mei, K. D. T. Ngo, and G. Lu, "Hetero-magnetic coupled inductor (HMCI) for high frequency interleaved multiphase dc/dc converters," in *Proc. IEEE Appl. Power Electron. Conf. Expo.*, Mar. 2019, pp. 2667–2672.
[7] J. Hu and C. R. Sullivan, "The quasi-distributed gap technique for planar inductors: Design guidelines," in *Proc. 32nd IAS Annu. Meeting Ind. Appl. Conf.*, Oct. 1997, vol. 2, pp. 1147–1152
[8] EPCOS AG—a TDK GroupCompany, "Distributed air gaps in ferrite cores," Jun. 2017. [Online]. Available: https://de.tdk.eu/download/2113422/321697054fce0c768ea66959fde3b3db/ferrites-air-gaps-pb.pdf
[9] Y. Cai, M. H. Ahmed, Q. Li, and F. C. Lee, "Optimized design of integrated PCB-winding transformer for MHz LLC converter," in *Proc. IEEE Appl. Power Electron. Conf. Expo.*, Mar. 2019, pp. 1452–1458.
[10] J. Schäfer, D. Bortis, and J. W. Kolar, "Optimal design of highly efficient and highly compact PCB winding inductors," in *Proc. IEEE 19th Workshop Control Model. Power Electron.*, Jun. 2018, pp. 1–8.
[11] S. Mukherjee, Y. Gao, and D. Maksimović, "Reduction of ac winding losses due to fringing-field effects in high-frequency inductors with orthogonal air gaps," *IEEE Trans. Power Electron.*, vol. 36, no. 1, pp. 815–828, Jan. 2021.
[12] A. J. Hanson and D. J. Perreault, "A high-frequency power factor correction stage with low output voltage," *IEEE Trans. Emerg. Sel. Topics Power Electron.*, vol. 8, no. 3, pp. 2143–2155, Sep. 2020.
[13] D. J. Perreault *et al.*, "Opportunities and challenges in very high frequency power conversion," in *Proc. 24th Annu. IEEE Appl. Power Electron. Conf. Expo.*, Feb. 2009, pp. 1–14.
[14] J. Hu, "Design of low-voltage, high-bandwidth radio frequency power converters," Ph.D. dissertation, Dept. Elect. Eng. Comput. Sci., Massachusetts Inst. Technol., Cambridge, MA, USA, 2012.
[15] T. H. Lee, *Planar Microwave Engineering: A Practical Guide to Theory, Measurement, and Circuits*, *1st ed*. Cambridge, U.K.: Cambridge Univ. Press, Aug. 2004, pp. 140–142.
[16] TDK, "Mn-Zn ferrite cores for switching power supplies, RM series," May 2019. [Online]. Available: https://product.tdk.com/info/en/catalog/datasheets/ferrite_mz_sw_rm_en.pdf
[17] Magnetics, "Ferrite pot cores," May 2019. [Online]. Available: https://product.tdk.com/info/en/catalog/datasheets/ferrite_mz_sw_rm_en.pdf
[18] C. R. Sullivan and R. Y. Zhang, "Simplified design method for litz wire," in *Proc. IEEE Appl. Power Electron. Conf. Expo.*, 2014, pp. 2667–2674.
[19] C. P. Steinmetz, "On the law of hysteresis," *Trans. Amer. Inst. Elect. Eng.*, vol. 9, no. 1, pp. 1–64, Jan. 1892.
[20] P. L. Dowell, "Effects of eddy currents in transformer windings," *Proc. Inst. Elect. Eng.*, vol. 113, no. 8, pp. 1387–1394, Aug. 1966.
[21] C. R. Sullivan, T. Abdallah, and J. Pollock, "Litzopt," Oct. 2019. [Online]. Available: http://power.thayer.dartmouth.edu/litzopt_init_web.html
[22] C. R. Sullivan, "Computationally efficient winding loss calculation with multiple windings, arbitrary waveforms, and two-dimensional or three-dimensional field geometry," *IEEE Trans. Power Electron.*, vol. 16, no. 1, pp. 142–150, Jan. 2001.
[23] D. Neumayr, D. Bortis, J. W. Kolar, S. Hoffmann, and E. Hoene, "Origin and quantification of increased core loss in MnZn ferrite plates of a multi-gap inductor," *CPSS Trans. Power Electron. Appl.*, vol. 4, no. 1, pp. 72–93, Mar. 2019.

Rachel S. Yang (Student Member, IEEE) received the B.S. and M.Eng. degrees in electrical engineering in 2018 and 2019, respectively, from the Massachusetts Institute of Technology, Cambridge, MA, USA, where she is currently working toward the Ph.D. degree.

Her research interests include magnetics design and modeling for high-frequency power electronics.

Alex J. Hanson (Member, IEEE) received the B.E. degree from Dartmouth College, Hanover, NH, USA, in 2014, and the S.M. and Ph.D. degrees from the Massachusetts Institute of Technology, Cambridge, MA, USA, in 2016 and 2019 respectively.

In 2019, he joined the University of Texas at Austin, Austin, TX, USA, where he is currently an Assistant Professor with the Department of Electrical and Computer Engineering. His research interests include power electronics, power magnetics, and their applications.

Dr. Hanson was the recipient of the William M. Portnoy Prize Paper Award in 2016.

Charles R. Sullivan (Fellow, IEEE) received the B.S. (hons.) degree from Princeton University, Princeton, NJ, USA, in 1987, and the Ph.D. degree from the University of California, Berkeley, CA, USA, in 1996, both in electrical engineering.

Between the B.S. and Ph.D. degrees, he was with Lutron Electronics Designing Electronic Ballasts. He is currently a Professor with the Thayer School of Engineering, Dartmouth College, Hanover, NH, USA, where he is also the Director of the Power Management Integration Center. He is a co-founder of Resonant Link, Inc. and holds 43 U.S. patents. His research interests include modeling and design optimization of magnetics and other passive components for high-frequency power conversion and wireless power transfer.

Dr. Sullivan was the recipient of the Power Electronics Society Modeling and Control Technical Achievement Award in 2018 and three IEEE Power Electronic Society Prize Paper Awards.

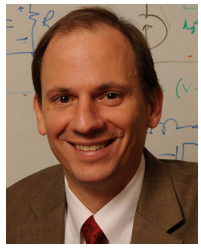

David J. Perreault (Fellow, IEEE) received the B.S. degree from Boston University, Boston, MA, USA, in 1989, and the S.M. and Ph.D. degrees from the Massachusetts Institute of Technology, Cambridge, MA, USA, in 1991 and 1997 respectively.

In 1997, he joined the MIT Laboratory for Electromagnetic and Electronic Systems, as a Postdoctoral Associate and then a Research Scientist in 1999. In 2001, he joined the MIT Department of Electrical Engineering and Computer Science, where he is currently the Joseph F. and Nancy P. Keithley Professor of Electrical Engineering. He also consults in industry and co-founded Eta Devices, Inc. (acquired by Nokia in 2016) and Eta Wireless, Inc., startup companies focusing on addressing efficiency challenges in radio frequency power amplifiers. He is a co-author of 13 IEEE prize papers. His research interests include design, manufacturing, and control techniques for power electronic systems and components, and their use in a wide range of applications.

Dr. Perreault is a member of the National Academy of Engineering. He received the Richard M. Bass Outstanding Young Power Electronics Engineer Award, the R. David Middlebrook Achievement Award, the Office of Naval Research Young Investigator Award, and the SAE Ralph R. Teetor Educational Award.